JMEPEG (2011) 20:1648–1657
DOI: 10.1007/s11665-011-9866-7

1059-9495/$19.00

Numerical Simulation and Experimental Validation of Residual Stresses in Water-Quenched Aluminum Alloy Castings

Bowang Xiao, Keyu Li, Qigui Wang, and Yiming Rong

(Submitted September 23, 2010; in revised form December 24, 2010)

Aluminum alloy castings are normally water quenched after solution treatment to improve mechanical properties. Rapid water quenching can result in high-residual stress and severe distortion which significantly affect functionality and performance of the products. To optimize product design and durability, one needs to model and predict residual stress and distortion produced in the water-quenched components. In this article, a finite element-based approach was developed to simulate the transient heat transfer and residual stress development during water quenching. In this approach, an iterative zone-based heat transfer algorithm was coupled with material constitutive model called mechanical threshold stress (MTS). With the integrated models, a good agreement was achieved between the numerically predicted and the experimentally measured residual stresses in the aluminum alloy frame-shape casting. The integrated FEA-based heat transfer and residual stress models were also applied to a water-quenched cast aluminum cylinder head with a great success.

Keywords aluminum alloy casting, finite element, heat treating, material constitutive model, residual stress, water quenching

1. Introduction

Aluminum alloy castings are widely used in automotive industry to improve fuel efficiency because of the high strength to weight ratio. Most of the aluminum alloy castings are quenched in water after solution treatment to improve mechanical properties such as tensile strengths and hardness. However, high-cooling rates in water quenching can produce significant amounts of residual stresses (Ref 1, 2) that can result in severe distortion (Ref 3), even cracking. Tensile residual stress produced during water quenching is also detrimental to fatigue properties of the material (Ref 2, 4). Therefore, product geometry design and heat-treatment processing must be optimized so that the mechanical properties can be improved and meanwhile residual stress and distortion are minimized. This can be achieved with the development of a numerical approach to accurate prediction of residual stress and distortion in the quenched components.

Because of the complexity of part geometry and boundary conditions and in particular the variation of material behaviors under different thermal and stress conditions, the numerical modeling of quenching process with any available finite element packages is still full of challenges. In this article, the problems in each stage of numerical simulation of quenching were analyzed and a reliable approach was developed. First, quenching experiments with target components were conducted to determine zone-based heat transfer coefficient (HTC) distribution data. Second, the optimized HTC data were applied to transient thermal analysis of the quenched castings with a finite element package, which generates temperature-time profile. Third, the structural analysis was performed to predict quenching results such as residual stress and distortion based on the temperature profile of the quenched casting and material constitutive model for aluminum alloy casting. A user material constitutive subroutine was developed and applied in the structural analysis. Finally, a validation of the finite element modeling was completed by measuring residual stresses using resistance strain gage rosette hole-drilling method. The good agreement of residual stresses between numerical predictions and experimental measurements indicates that the numerical simulation approach developed and used in this article provides accurate results.

Bowang Xiao and **Yiming Rong**, Manufacturing Engineering, Worcester Polytechnic Institute, Worcester, MA 01609; **Keyu Li**, Mechanical Engineering, Oakland University, 103 Dodge Hall, Rochester, MI 48309; and **Qigui Wang**, Global Product Engineering, General Motors Company, Pontiac, MI 48340. Contact e-mail: bowangxiao@gmail.com.

2. Numerical Simulation Approach

Numerical simulations of heat transfer and residual stress of metal parts can be carried out using the finite element method. Figure 1 illustrates a proposed procedure of numerical simulation of quenching process. A CAD geometry model of the part is created in 2-D or 3-D form and then meshed with suitable elements. The temperature-displacement simulation is decoupled to thermal simulation and structural simulation for fast convergence and low-computational cost since the heat generated by deformation during quenching is negligible compared to the heat transferred from hot solid to environmental media. Thus, thermal simulation is first carried out to

obtain temperature-time profile of the part. The subsequent structural simulation reads the temperature-time profile and predicts residual stress and distortion profiles. In order to ensure high-accurate simulation results, the finite element modeling is finally validated by experimental measurements.

The thermal simulation of heat treating is a transient temperature analysis, in which the temperature of the hot part changes with respect to time from an initial state to a final state. In this simulation, it is usually easy to obtain and assign reasonably accurate data to initial temperature of the hot part and temperature of quenchant, as well as the thermophysical properties of the part material. The biggest uncertainty is the HTC between the hot part and quenchant. It has been reported that HTC affects the quenching results significantly (Ref 3, 5). In liquid quenching, the heat transfer between hot aluminum alloy castings and liquid is very complicated and difficult to be determined analytically. When a hot part is quenched in a fluid such as oil or water, the heat transfer usually consists of three stages: film boiling stage, nucleate boiling stage, and convection stage (Ref 6). The intense interactions between hot solid and cold fluid lead to a very complicated heat transfer process (Ref 6, 7). As a result, efforts need to be put on acquiring HTC distribution for a specific part as real as possible. Empirical equations might be used to determine the HTC, but the big difference between calibration condition of empirical equations and production condition of quenching can lead to an uncertainty as high as 25% (Ref 8). Experiments with small probe might be conducted to determine HTC (Ref 6, 9, 10), but with this method it is very difficult to take the complicated geometry of a real part into consideration. Even with the state-of-the-art CFD packages, it is impossible to accurately simulate the interaction between hot solid and cold liquid. Therefore, it is proposed to use zone-based HTC approach for water quenching of aluminum alloy casting, which is demonstrated in Section 3 of this article.

In the structural simulation, the temperature-time profile of the quenched work piece from the thermal simulation is read in. The finite element code then calculates local (node to node) displacements based on the temperature distribution and the relevant materials properties. During quenching, the part shrinks because of the temperature drop. The nonuniform thermal shrinkage of the part is constrained by the geometric structure and material properties that vary with temperatures and strain rates (Ref 2, 11-13). Thus, an accurate representation of the material behavior at different temperatures and strain rates is extremely important to the simulation results. This can be done by applying multiple stress-strain curves for different temperatures and strain rates in the finite element analysis to govern the material constitutive behavior during quenching (Ref 2). However, the linear interpolation of the material constitutive relationship at other temperatures and strain rates between these curves can introduce errors. Section 4 of this article introduces the material constitutive model used in the numerical simulation.

To evaluate the accuracy and applicability of the integrated residual stress models, the predicted results such as residual stress and distortion can be compared with experimental measurements. In this work, residual stresses at certain locations of the water-quenched castings were measured and used to validate simulation accuracy (Ref 2, 4). There are many different methods to measure residual stresses such as x-ray diffraction, neutron diffraction, resistance strain gage hole-drilling method, curvature and layer removal methods, magnetic method, and ultrasonic method (Ref 14). In this article, residual stresses were measured using the most widely applied method (Ref 15), resistance strain gages center hole-drilling method described in the ASTM standard E837 (Ref 16). The central hole-drilling method can provide residual stress distribution in the depth direction, which is good for the model validation. In addition, this method is reliable, cheap, and also easy to use. Section 5 of this article illustrates the simulation predictions and section 6 compares the predicted residual stresses with experimental measurements.

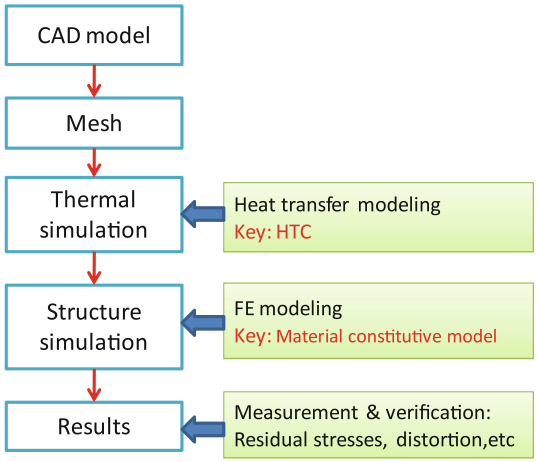

Fig. 1 Illustration of numerical simulation and experimental validation procedures for residual stress prediction

3. Heat Transfer Modeling

The thermal simulation is to obtain temperature-time profile of the quenched part. As mentioned above, heat flux and HTC data vary from location to location and play very important roles in affecting quenching results. In this article, an aluminum alloy frame-shape casting was quenched at the orientation shown in Fig. 2. The casting was instrumented with multiple thermocouples to acquire temperature-time curves at various

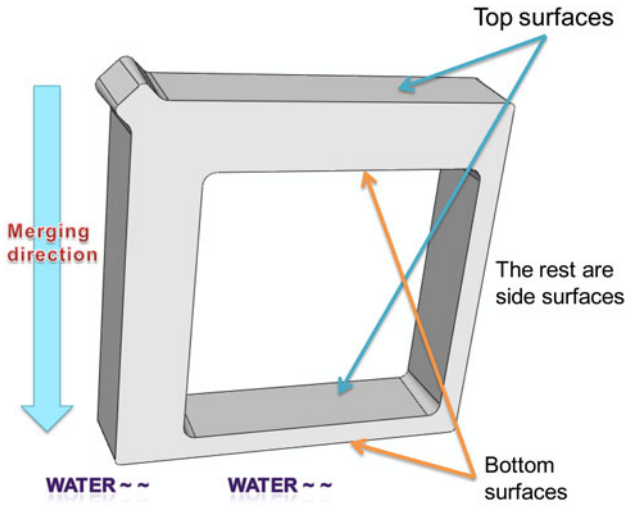

Fig. 2 Surface grouping

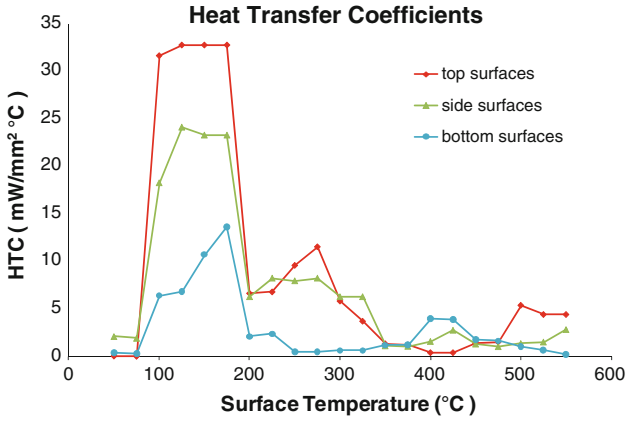

Fig. 3 HTC vs. surface temperature

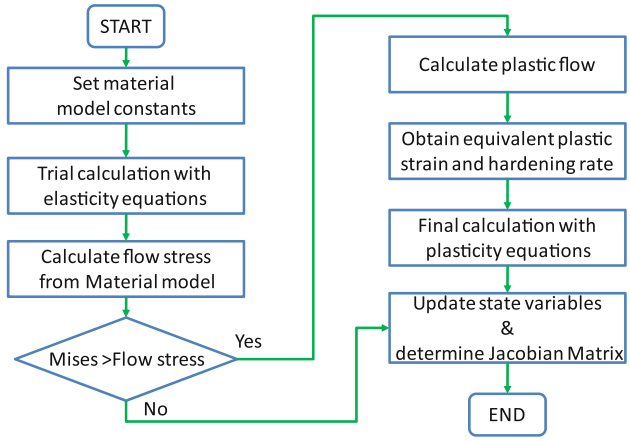

Fig. 4 Flow chart of UMAT

locations during quenching. The surfaces of the casting with similar quench orientation were grouped together as one zone as shown in Fig. 2 and it is assumed there is only one uniform HTC curve for each zone. In HTC optimization, initial HTC data were assigned to each zone and a thermal simulation was conducted to obtain temperature-time curves at the locations where thermocouples were instrumented. The HTC data were then modified based on the differences between the simulated temperatures and the experimentally measured temperatures. Another simulation was then conducted with the modified HTC and the HTC data were modified again based on the simulation results. After several iterations, the HTC data converge to some values when the temperature differences between simulation and experiment fall into an accepted tolerance such as 5 °C. Accordingly, the optimized zone-based HTC data for the frame-shape casting were determined, which were illustrated in Fig. 3 (Ref 17).

4. Material Constitutive Model

To accurately predict quenching results, the temperature- and strain rate-dependent material constitutive behavior needs to be modeled. Following Newman et al., a material constitutive model called mechanical threshold stress (MTS), was adapted in this work for water quenching process (Ref 11). In this model, the flow stress σ is the sum of two components: an "intrinsic strength" σ_i and a state variable σ_e. The intrinsic strength σ_i models yielding and σ_e evolves with the deformation to model hardening. The flow stress is expressed as Eq 1.

$$\frac{\sigma}{\mu(T)} = S_i(\dot{\varepsilon}, T)\frac{\hat{\sigma}_i}{\mu_0} + S_e(\dot{\varepsilon}, T)\frac{\hat{\sigma}_e}{\mu_0} \quad \text{(Eq 1)}$$

Here, $\mu(T)$ is the temperature-dependent shear modulus, expressed as

$$\mu(T) = \mu_0 - \frac{3440}{\exp\left(\frac{215}{T}\right) - 1}, \quad \text{(Eq 2)}$$

where $\mu_0 = 28.815$ GPa is the reference value at 0 K, $\dot{\varepsilon} = 10^7/\text{s}$, and T is the temperature in Kelvin.

At the yielding point, $\hat{\sigma}_e = 0$. After yielding, a linear form of the state variable is used in this model as expressed in Eq 3.

$$\hat{\sigma}_e = \hat{\sigma}'_e + \frac{\mu(T)}{\mu_0}\theta_0\left[1 - \frac{\hat{\sigma}'_e}{\hat{\sigma}_{os}}\right]d\varepsilon, \quad \text{(Eq 3)}$$

where θ_0 represents the slope of the stress-strain curve at yield in the reference state ($0\,\text{K}\ \dot{\varepsilon} = 10^7/\text{s}$). $\hat{\sigma}_{os}$ is a material parameter, $\hat{\sigma}'_e$ is the previous state variable, and $d\varepsilon$ is the strain increment during the evolution.

Velocity-modified temperatures, $S_i(\dot{\varepsilon}, T)$ and $S_e(\dot{\varepsilon}, T)$, are used to scale the temperature and strain rate as following:

$$S_i(\dot{\varepsilon}, T) = \left[1 - \left[\frac{kT}{\mu(T)b^3 g_{oi}}\ln\left(\frac{\dot{\varepsilon}_0}{\dot{\varepsilon}}\right)\right]^{\frac{1}{q_i}}\right]^{\frac{1}{p_i}} \quad \text{(Eq 4)}$$

$$S_e(\dot{\varepsilon}, T) = \left[1 - \left[\frac{kT}{\mu(T)b^3 g_{oi}}\ln\left(\frac{\dot{\varepsilon}_0}{\dot{\varepsilon}}\right)\right]^{\frac{1}{q_e}}\right]^{\frac{1}{p_e}}, \quad \text{(Eq 5)}$$

where g_{oi} and g_{os} are the activation energy for flow at yielding and saturation, respectively. They are normalized by Boltzmann's constant, k, the Burgers vector, b, and the shear modules, $\mu(T)$.

The constants p_i, q_i, p_e, and q_e are related to the interaction of dislocations with precipitates. The values of those constants can be found in Newman's paper (Ref 11).

Young's modulus is determined from the stress-strain curves of tensile tests at different temperatures and strain rates and is fitted to a second-order polynomial as expressed in Eq 6.

$$E = 67,599 + 72.353T - 0.14767T^2 \quad \text{(Eq 6)}$$

In this material constitutive model, all other parameters are treated as constants, except the four parameters: $\hat{\sigma}_{os}$, $\hat{\sigma}_i$, g_{oi}, and g_{os}, which can be determined from tensile tests at various temperatures and strain rates for the specific material.

To apply the material constitutive model in the finite element simulations, a user subroutine UMAT was programmed in FORTRAN language (Ref 18) for FE package ABAQUS (Ref 19). During simulation, the FEA code calls UMAT at each integration point to construct the stiffness matrix. As shown in the flow chart in Fig. 4, for every call at each point, UMAT first conducts a trial elastic calculation with the inputs (previous status, strain increments, temperature, etc.) from FEA code and generates the new status of stress, strain, etc. The subroutine then compares the Von Mises of the trial calculation with the flow stress predicted by the MTS material model to see if there

is any plastic flow in this increment. If there is no plastic flow, the subroutine updates the state variables and returns the Jacobian matrix to FEA code for global calculation. If there is plastic flow, the subroutine recalculates the new status with plastic theory and updates the state variables and Jacobian matrix. The Jacobian matrix governs the evolution of material behaviors. The calculation of new status with plastic theory usually cannot be done in one step because of the nonlinear characteristics and is usually done iteratively.

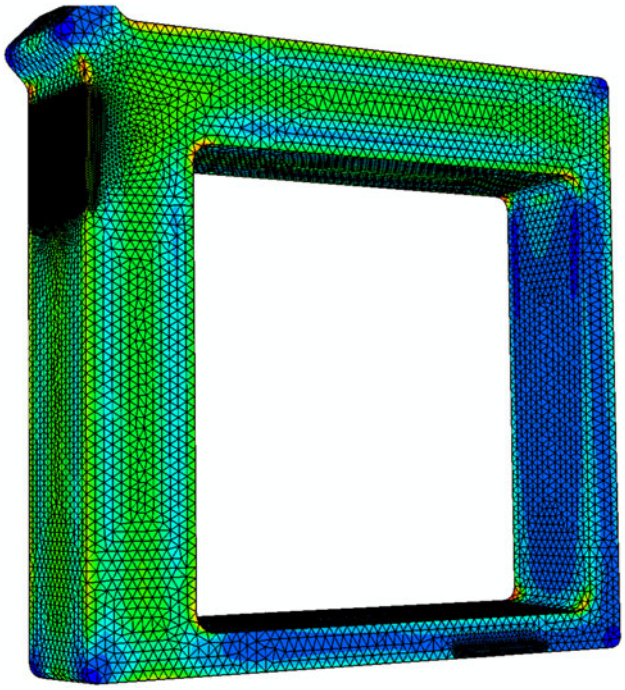

Fig. 5 The meshed casting frame

5. Model Validation

The model validation was carried out with a water-quenched aluminum alloy frame-shape test casting. Figure 5 shows the FEA mesh of the casting. In the mesh scheme, the elements in residual stress measurement areas (dark area in Fig. 5) are 0.5 mm in size and the rest elements are 2 mm in size. In this scheme, there are 432,714 second-order tetrahedral elements and 611,088 nodes for the casting. In the FE model, experimentally obtained zone-based HTC data described in Section 3 were used to govern the thermal boundary conditions of the casting. No external forces or constrains were applied to the casting except for those three point constraints to remove the free body movement. Material constitutive model, in the form of user subroutine UMAT, was applied in the structural analysis.

The predicted residual stresses at two locations in both thick and thin legs were selected for comparison with measurements. Figure 6 shows the predicted residual stresses at the measurement area on the thick leg. Table 1 tabulates the three nodes chosen at different depths at the measurement point and their corresponding residual stresses in the YOZ plane. Figure 7 shows the predicted residual stresses at the measurement area on the thin leg. Table 2 illustrates the three nodes chosen at different depths at the measurement point and residual stresses in the XOZ plane. It is seen that on the thick leg normal stresses are negative (compressive) in both y and z directions and the shear stress is negligible compared to the normal stresses. On the thin leg, normal stress is negative in Z direction and positive (tensile) in X direction. Compressive residual stresses are usually expected at surfaces of quenched parts because inside of the part cools much more slowly than the surfaces. In the frame-shape casting, the thin leg is cooled faster than the thick leg due to the volume difference. When the thick leg is cooled down, the cold thin leg is tensioned and therefore a tensile stress was produced on the thin legs.

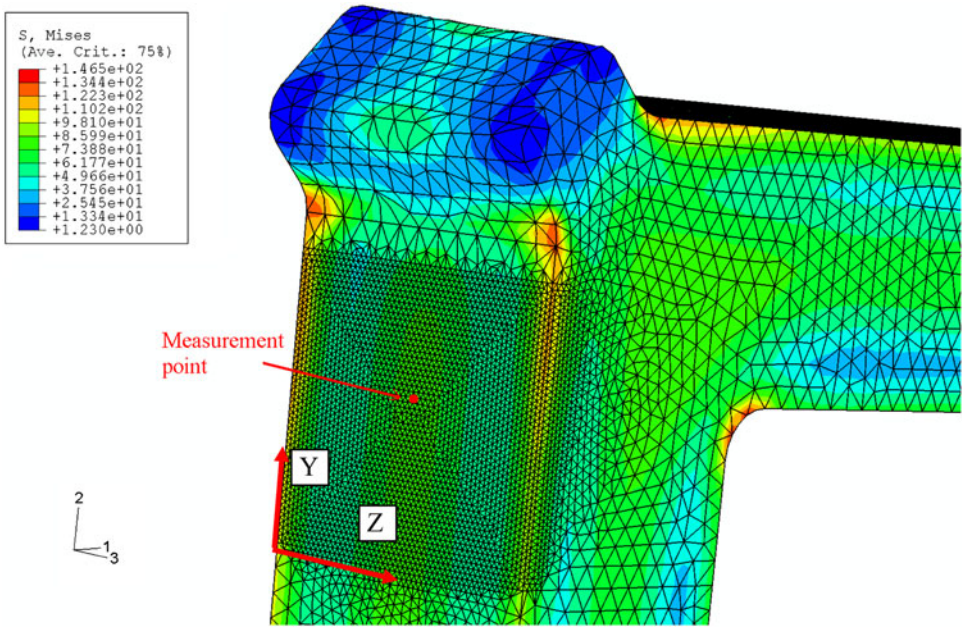

Fig. 6 Residual stresses on thick leg

Table 1 Nodes on thick leg

Node ID	*x*, mm	*y*, mm	*z*, mm	σ_{yy}, MPa	σ_{yz}, MPa	σ_{zz}, MPa	Depth from surface, mm
534,198	0.804	99.571	12.217	−47.198	−0.160	−69.067	0
498,904	1.302	99.571	12.468	−28.569	−0.014	−43.775	0.5
497,259	1.806	99.896	12.656	−14.433	−0.071	−25.342	1

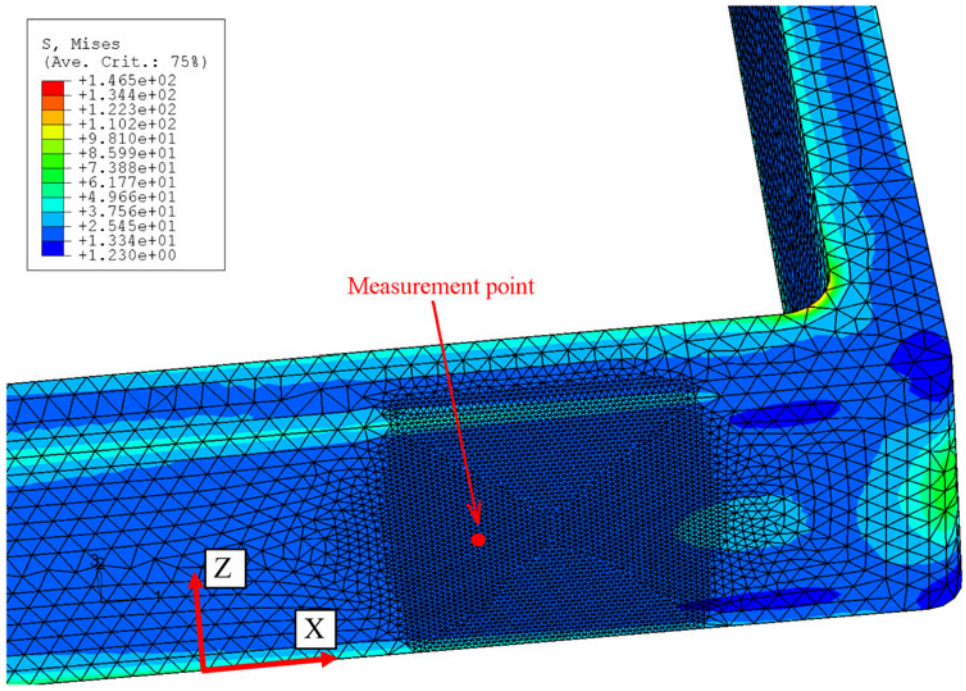

Fig. 7 Residual stresses on thin leg

Table 2 Nodes on thin leg

Node ID	*x*, mm	*y*, mm	*z*, mm	σ_{xx}, MPa	σ_{xz}, MPa	σ_{zz}, MPa	Depth from surface, mm
293,411	86.450	0.574	12.500	34.296	−1.524	−22.934	0
254,109	86.349	1.097	12.549	32.704	−1.322	−13.083	0.5
218,700	86.448	1.560	12.403	31.422	−1.016	−6.701	1

To validate the model predictions, residual stresses at the two locations of the test casting were measured using resistance strain gage rosette hole-drilling method. A strain gage rosette was first mounted onto the surface of the sample, and a small hole was drilled at the center of the three strain gages. During the hole-drilling, strains were relieved due to the release of residual stresses. The relieved strains were measured and used to back-calculate residual stresses in that small area using Eq 7.

$$\begin{bmatrix} \sigma_1 \\ \tau_{13} \\ \sigma_3 \end{bmatrix} = \begin{bmatrix} A+B, & 0, & A-B \\ A, & -2B, & A \\ A-B, & 0, & A+B \end{bmatrix}^{-1} \begin{bmatrix} \varepsilon_1 \\ \varepsilon_2 \\ \varepsilon_3 \end{bmatrix}, \qquad \text{(Eq 7)}$$

where the relieved strains in three directions were measured using three strain gages (#1, #2, and #3), and the coefficients matrix (CM) is constructed from the coefficients A and B. In practice, the hole is drilled layer by layer so that residual stresses at different layer (depth) can be determined. An integral method (Ref 15) was proposed to better predict stress distribution especially for a nonuniform stress field. In the back calculation of residual stresses from the relived strains during measurement, the way to improve the accuracy of the measurements by applying calibration coefficients specially obtained for a specific measurement (Ref 20) was used.

The residual stress measurement setup is shown in Fig. 8. To reduce the experimental error, the measurements at each location were repeated three times. Some samples after measurements are shown in Fig. 9.

Because of the geometric symmetry, the maximum principle residual stresses on the surfaces of the measured areas are in the longitudinal and latitude directions as mentioned in the simulation section. The residual stresses in the depth direction are very small. Figures 10-13 show the means, upper and lower bounds of the experimentally measured principle residual

stresses at those two locations. It is seen that the predicted residual stresses in both Y and Z directions agree with the measurements especially at depths ranging from about 0.5 to 1 mm. There is a slight discrepancy near the surface. This is probably due to the relaxation from surface preparation for mounting the resistance strain gage rosettes. Similar observations are obtained for thin legs in Fig. 12 and 13.

Due to the nature of being not measurable directly and variation of residual stress with time and temperature, it is usually of big challenges to measure residual stress in a very accurate manner. The strain gage center hole-drilling integral method applied in this article is considered as a cheap and accurate method, the accuracy of which can be in the order of 1 MPa. However, the measurement preparation (surface cleaning for mounting strain gages) will introduce some measurement errors. During the measurement, there are some local

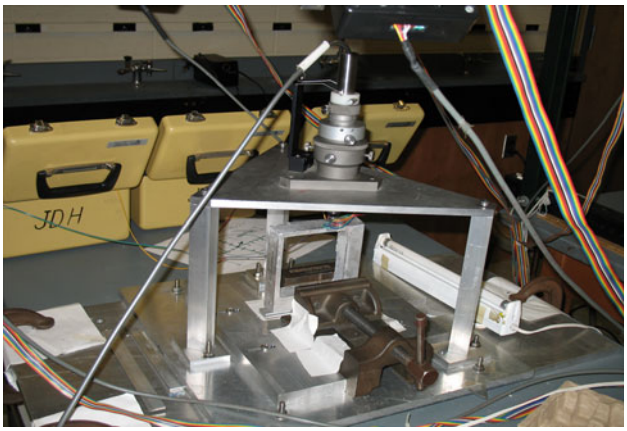

Fig. 8 Residual stress measurement setup

Fig. 9 Residual stress measurement locations on the castings

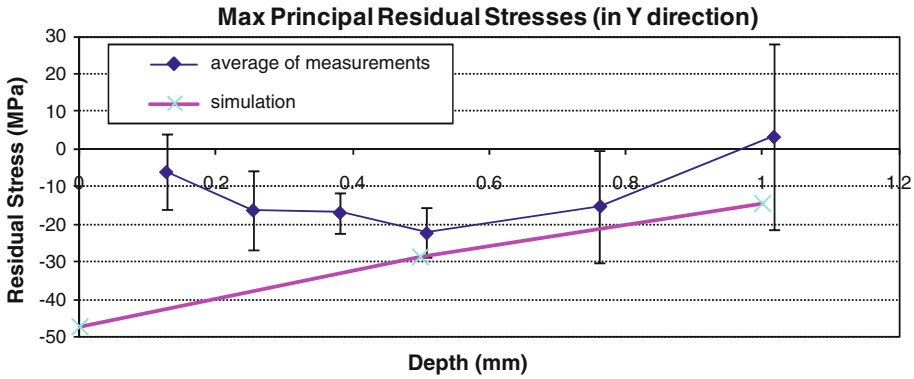

Fig. 10 Comparison of maximal principal residual stress at thick leg

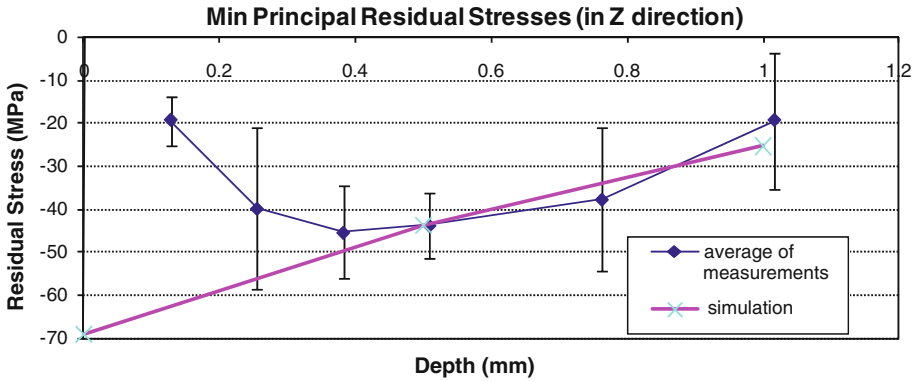

Fig. 11 Comparison of minimal principal residual stress at thick leg

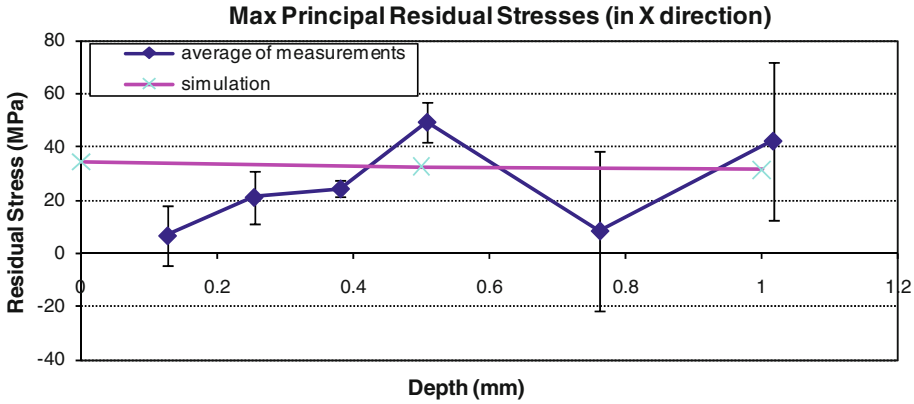

Fig. 12 Comparison of maximal principal residual stress at thin leg

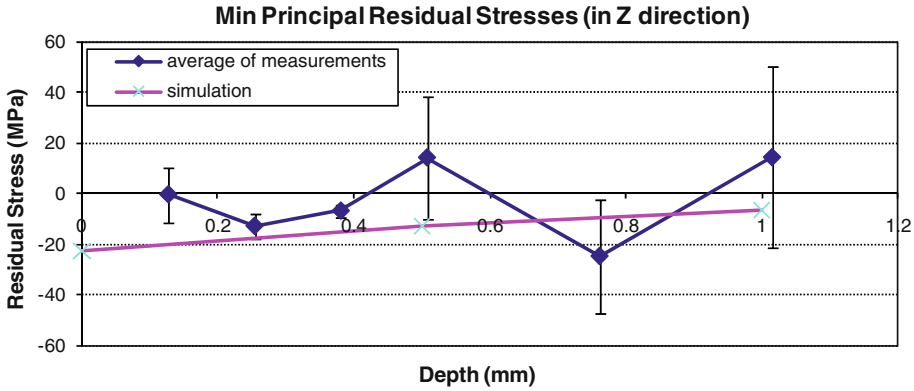

Fig. 13 Comparison of minimal principal residual stress at thin leg

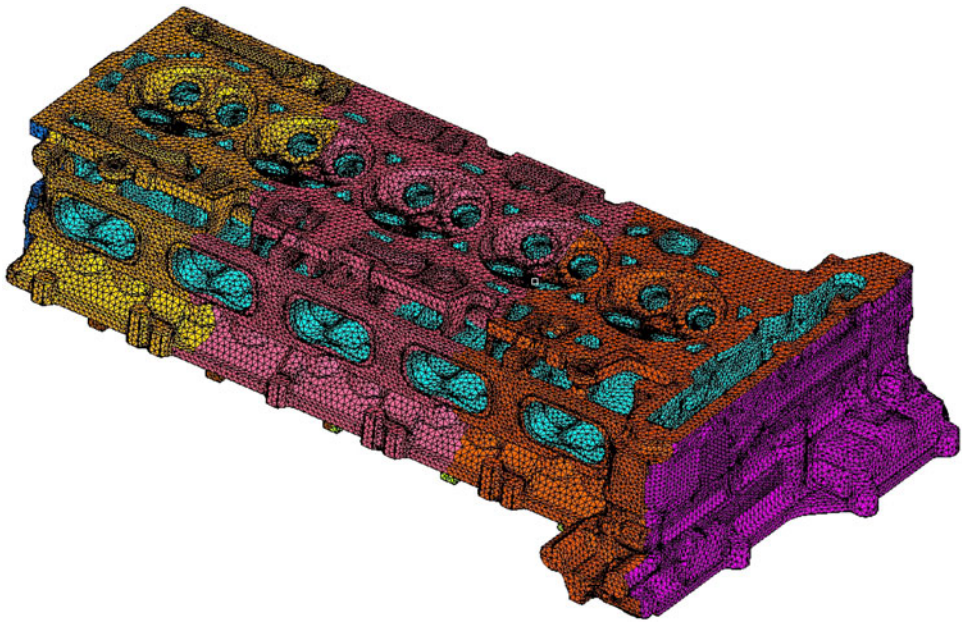

Fig. 14 Meshed cylinder head

temperature changes in the measurement area due to drilling the hole. The local temperature change can cause a strain change, which must be eliminated from the strain change caused by the hole-drilling (local stress release). Waiting before recording strain data till they are stable can help reduce the temperature-introduced strains, but it is difficult to remove the phase

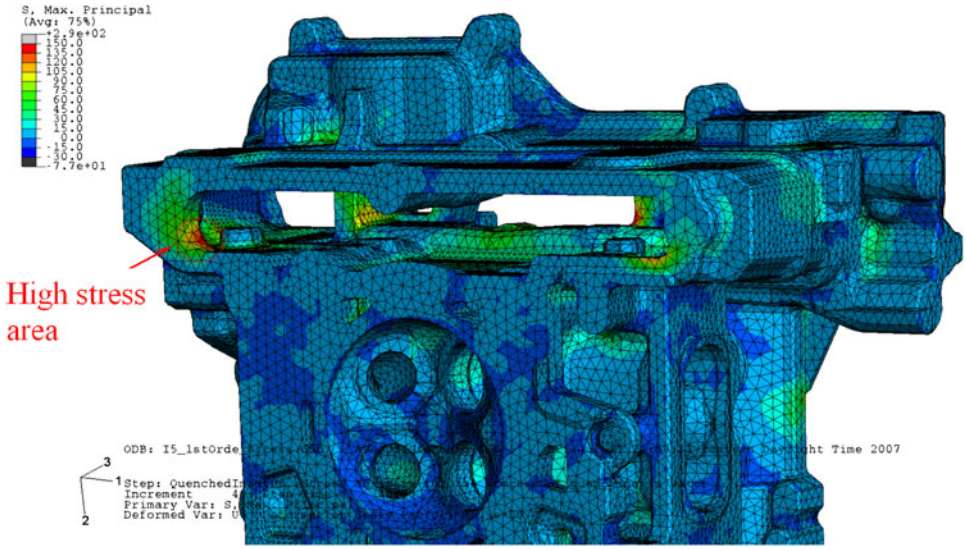

Fig. 15 High-residual stress predicted at cracking area

Fig. 16 Residual stress measurement locations on cylinder head

transformation introduced strains due to the aging effect of aluminum alloy at relatively high temperatures. It is also noticed that the numerical simulation can introduce some certain of errors due to the mesh, zone-based HTC data, etc. The node-based HTC data can be obtained by integral application of CFD simulation and experimental measurement and can improve simulation accuracy (Ref 21). In general, as we can see from these figures, the numerical predictions are in a good agreement with measurements, indicating that these material models and HTC data are good for industrial applications.

6. Model Applications

The validated residual stress models were applied to a water-quenched cylinder head. Figure 14 shows the cylinder head

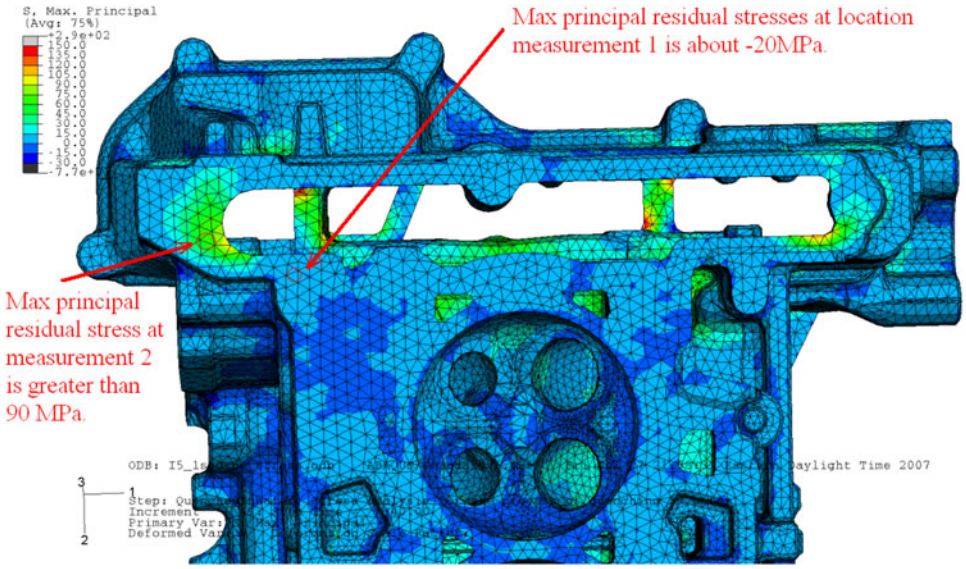

Fig. 17 Maximal principal residual stresses

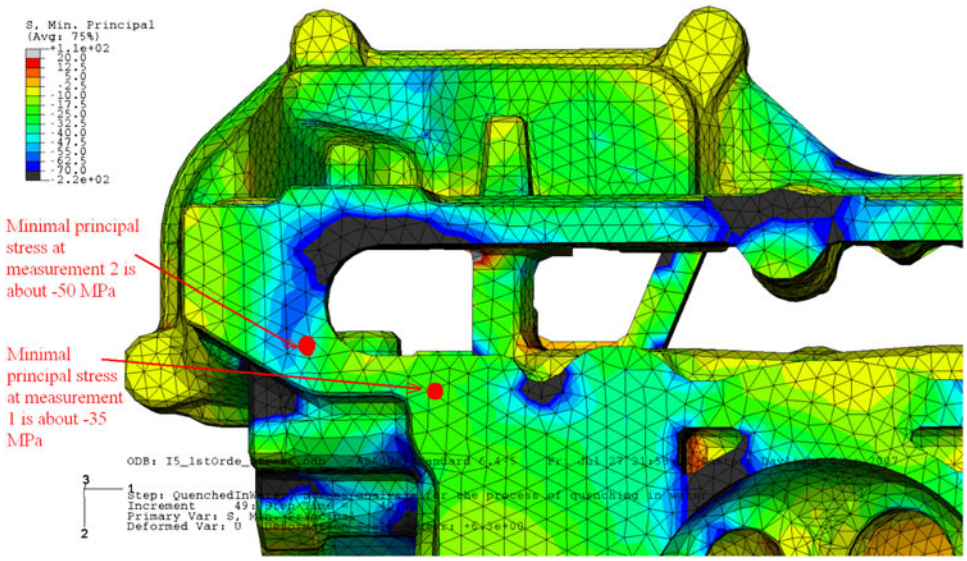

Fig. 18 Minimal principal residual stresses

Table 3 Comparison of residual stresses on cylinder head

	Location 1		Location 2	
Note: approximated data were used	**Max principal stress, MPa**	**Min principal stress, MPa**	**Max principal stress, MPa**	**Min principal stress, MPa**
Simulation	−10	−30	80	−48
Measurement	−20	−35	90	−50

geometry and FEA mesh. The mesh scheme consists of 1,089,515 tetrahedral elements and 1,757,074 nodes with the element size ranging from 5 to 10 mm. In practice, the cylinder head was quenched vertically in warm water after solution treatment. High-residual stresses were observed in the location marked "high-stress area" in Fig. 15. To evaluate the accuracy of the predictions, the residual stresses at the location near the high-stress area, shown in Fig. 16, were also measured.

The predicted maximal and minimal principal residual stresses near the locations 1 and 2 are shown in Fig. 17 and 18, respectively. A comparison of the predicted and measured residual stresses at the locations 1 and 2 are shown in Table 3. It can be seen that the predictions are in good agreement with the measurements.

7. Conclusions

In this article, a numerical approach to simulating residual stress and distortion in the water-quenched aluminum alloy castings was put forward. An iterative zone-based heat transfer algorithm was developed to simulate the transient heat transfer of aluminum casting during quenching. A material constitutive model called MTS was adapted and calibrated in the model to calculate the material behavior with respect to different temperatures and strain rates. The developed residual stress model, validated with a simple shape test casting, can be used to predict residual stress and distortion of complex shape aluminum castings during quenching with high accuracy. The model was successfully used to predict residual stress during quenching of a cylinder head. The numerical simulation results agree with the experimental measurement results.

Acknowledgments

This work was supported financially by PowerTrain, General Motors Company, MI, USA. Dr. Bing Li from GM PowerTrain helped with meshing the cylinder head.

References

1. K. Li, B. Xiao, and Q. Wang, Residual Stresses in As-Quenched Aluminum Castings, *SAE Int. J. Mater. Manuf.*, 2009, **1**(1), p 725–731
2. P. Li, D.M. Maijer, and T.C. Lindley, Simulating the Residual Stress in an A356 Automotive Wheel and Its Impact on Fatigue Life, *Metall. Mater. Trans. B*, 2007, **38**(4), p 505–515
3. A. Rose, O. Kessler, and F. Hoffmann, Quenching Distortion of Aluminum Castings-Improvement by Gas Cooling, *Materialwiss. Werkst.*, 2006, **37**(1), p 116–121
4. Y.L. Lee, J. Pan, and R. Hathaway, *Fatigue Testing and Analysis: Theory and Practice*, Elsevier Butterworth-Heinemann, Burlington, 2005, p 402
5. Z. Li, R.V. Grandhi, and R. Srinivasan, Distortion Minimization during Gas Quenching Process, *J. Mater. Process. Technol.*, 2006, **172**(2), p 249–257
6. G.E. Totten, C.E. Bates, and N.A. Clinton, *Handbook of Quenchants and Quenching Technology*, ASM International, Materials Park, OH, 1993, p 514
7. M. Sedighi and C.A. McMahon, The Influence of Quenchant Agitation on the Heat Transfer Coefficient and Residual Stress Development in

the Quenching of Steels, *Proc. Inst. Mech. Eng. B J. Eng. Manuf.*, 2000, **214**(7), p 555–567
8. J.P. Holman, *Heat Transfer*, McGraw-Hill, New York, 2002, p 665
9. M. Maniruzzaman, J. Chaves, and C. McGee, CHTE Quench Probe System: A New Quenchant Characterization System, *5th International Conference on Frontiers of Design and Manufacturing (ICFDM)*, 2002, p 619–625
10. D.K. Funatani, M. Narazaki, and M. Tanaka, Comparisons of Probe Design and Cooling Curve Analysis Methods, *19th ASM Heat Treating Society Conference Proceedings Including Steel Heat Treating in the New Millennium*, G. Krauss, S.J. Midea, and G.D. Pfaffmann, Ed., ASM International, Cincinnati, OH, 1999, p 255–263
11. M.L. Newman, B.J. Robinson, and H. Sehitoglu, Deformation, Residual Stress, and Constitutive Relations for Quenched W319 Aluminum, *Metall. Mater. Trans. A*, 2003, **34**(7), p 1483–1491
12. H. Sehitoglu, T. Smith, and X. Qing, Stress-Strain Response of a Cast 319-T6 Aluminum Under Thermomechanical Loading, *Metall. Mater. Trans. A*, 2000, **31**(1), p 139–151
13. C.M. Estey, S.L. Cockcroft, and D.M. Maijer, Constitutive Behaviour of A356 During the Quenching Operation, *Mater. Sci. Eng. A*, 2004, **383**(2), p 245–251
14. J. Lu and M. James, *Handbook of Measurement of Residual Stresses*, Fairmont Press, Inc, Lilburn, GA, 1996, p 237
15. G.S. Schajer, Measurement of Non-Uniform Residual Stresses Using the Hole-Drilling Method. Part I-Stress Calculation Procedures, *J. Eng. Mater. Technol.*, 1988, **110**, p 338–343
16. ASTM Designation: E837-01, ASTM International, Philadelphia, PA, 2002, p 703–712
17. B. Xiao, Q. Wang, and P. Jadhav, An Experimental Study of Heat Transfer in Aluminum Castings During Water Quenching, *J. Mater. Process. Technol.*, 2010, **210**(4), p 2023–2028
18. Compaq Inc., Fortran, Version 6.6, TX, USA, 2002
19. ABAQUS Inc., ABAQUS Help Documentation, Version 6.7, Providence, RI, 2007
20. B. Xiao, K. Li, and Y. Rong, Automatic Determination and Experimental Evaluation of Residual Stress Calibration Coefficients for Hole-Drilling Strain Gage Integral Method, *Strain*, 2010, doi: 10.1111/j.1475-1305.2009.00650.x
21. B. Xiao, Q. Wang, G. Wang, R.D. Sisson, and Y. Rong, Robust Methodology for Determination of Heat Transfer Coefficient Distribution in Convection, *Appl. Therm. Eng.*, 2010, **30**(17), p 2815–2821